BULLETIN OF THE POLISH ACADEMY OF SCIENCES
TECHNICAL SCIENCES, Vol. 73(5), 2025, Article number: e155036
DOI: 10.24425/bpasts.2025.155036



# Full floating structure underwater explosion with pulsation and cavitation effect FEM simulation case

**Leszek FLIS***

Fundamentals of Ship Machinery Construction Department, Mechanical and Electrical Engineering Faculty,
Polish Naval Academy, Śmidowicza 69, 81-127 Gdynia, Poland

**Abstract.** This paper investigates the response of a floating structure to an underwater explosion, with particular focus on pulsation effects, using Finite Element Method (FEM) simulation. An extensive literature review revealed no accurate numerical studies addressing this specific scenario in peer-reviewed scientific publications. The results of a study on the impact of an initial shock wave on a floating structure, followed by a subsequent bubble shock wave caused by close underwater explosion, were presented. The findings illustrate the immediate effects of an underwater explosion near a floating structure, including the resulting shock wave and structural deformation. The formation of the bubble shock wave from the explosion-generated gas and the consequent deformation of the floating structure is detailed. Additionally, the phenomena such as cavitation that occur following the re-expansion of explosion-generated gas after the bubble shock wave is examined. This study, conducted using LS-DYNA, showcases the software's comprehensive capability to tackle these issues.

**Keywords:** UNDEX; underwater explosion; detonation; blast; cavitation; pulsation; FEM simulation; LS-DYNA.

## 1. INTRODUCTION

Underwater explosions (UNDEX) threaten ship hulls through complex dynamic loads. They produce intense, short-duration shock waves followed by prolonged bubble pulsations [1]. While the initial shock wave causes localized damage, subsequent pulsations may induce broader whipping effects and structural failure [2, 3]. In near-field cases, bubble collapse can also generate high-velocity jets, intensifying the damage.

To better understand and predict the consequences of UNDEX events on ships, researchers have conducted extensive experimental and numerical studies. Early work by Cole [1] and Geers [2] laid the foundation for modelling underwater shock waves and their effects. Subsequent studies focused on bubble dynamics [3], response characterization [4, 5], and damage mechanisms [6]. While many researchers have examined the overall structural response using hull girder models, localized damage, particularly at the bottom of ship hulls, remains less explored [7, 8].

Recent studies have indicated that detonation distance plays a critical role in determining damage severity. Investigations by Gan *et al*. [9] and He *et al*. [10] suggest that the interaction between shock waves, bubble collapse, and hull deformation is highly non-linear. Additionally, while the strain response and plastic deformation of ship hulls under UNDEX loads have been examined [11], the loss of total longitudinal strength remains insufficiently characterized [12]. Consequently, further research is needed to assess the full-scale effects of UNDEX on ship structures, particularly in terms of localized deformation and residual strength degradation.

In the past, several UNDEX experiments (Fig. 1, 2), particularly those conducted in the far field, both with and without the presence of a floating structure, were documented, and the studies are publicly available [15, 16]. These experiments successfully confirmed the pulsation phenomenon and the behaviour of gas bubbles generated by the explosions, as well as their impact on submerged objects. The theoretical foundations of UNDEX research were first established in 1948 [1] and have since been progressively refined through experimental and numerical advancements over subsequent decades. Currently, a comprehensive and detailed review of the classification of the effects of underwater explosions on ships can be found in [17], where

**Fig. 1.** Far field UNDEX. USS Winston Churchill DDG 81 Ship Shock Trial 2001 [13]

*e-mail: l.flis@amw.gdynia.pl

Manuscript submitted 2025-02-11, revised 2025-03-27, initially accepted for publication 2025-07-02, published in August 2025.

**Fig. 2.** Close field UNDEX. Australian Navy MK 46 Torpedo Test under keel [14]

FEM direct and acoustic methods were extensively studied concerning UNDEX. Beyond the classical UNDEX theory [1], the work in [18] offers a comprehensive approach to ship shock modelling.

Theoretical analysis, numerical simulations, and experiments are crucial for understanding UNDEX phenomena. These can be categorized into high-pressure electrical discharge tests [19], small-scale explosions [20], and large–scale field trials [17,21].

Conducting large-scale real-world experiments with underwater explosions encounters significant challenges, namely the lack of facilities for large tests. It is difficult to carry out experiments with large quantities of explosives (over 100 kg of TNT) in underwater conditions, making it challenging to meet the requirements for simulation validation. Nevertheless, real-world experiments range from miniature [22] to large-scale [23].

In most cases, UNDEX analytical solutions cannot be obtained, which necessitates the development of numerical models and methods to solve them, particularly FEM. There are relatively mature numerical methods for underwater explosions, such as quasi-static FEA [24] – applicable only if the equipment can be considered rigid, design response spectra (DRS) or dynamic design analysis method (DDAM) [25], dynamic or non-linear structural FEA, and presented here advanced numerical methods – e.g., fluid-structure interaction (FSI) [26].

Underwater explosions in the near field are associated with complex mechanical problems, particularly regarding their impact on structural damage and protection [27]. The near field, however, presents even greater challenges, as the dynamics of gas bubbles become significantly more intricate near the water surface or other obstacles. To accurately predict the behaviour of these bubbles and their effects on the surrounding environment, numerical modelling plays a crucial role.

Recently, there has been a renewed focus on close-field UNDEX simulations, driven by the increasing availability of high computational power, with China taking a leading role in this area. The literature review identified only two works [19,23] (by the same authors, effectively constituting one study) that present a similar numerical topic, but they do not provide many details for FEM solution.

The mentioned works, along with others, address the topic of UNDEX both from the experimental side and through FEM simulations [28–31]. With UNDEX FEM analysis a common denominator, they mainly concern far-field underwater explosions and generally do not take into account the added mass effect or the physical impact of gas bubble pulsations on the loading of the floating structure.

The aim of the article is to analyze the impact of underwater explosions (UNDEX) on floating structures, with particular emphasis on pulsation and cavitation effects. The study focuses on the numerical modelling of these phenomena using the finite element method (FEM) in LS-DYNA to better understand the mechanisms of shock wave interaction and the behaviour of explosion-generated gas bubbles affecting floating structures. Specifically, it seeks to determine the extent of structural deformations and compare the simulation results with existing theoretical models. The article addresses a research gap in the field of close-field UNDEX explosions, offering an innovative approach to the analysis of dynamic interactions in such an environment.

The author predicts, based on an analysis of literature encompassing over 240 sources, that the presented solution is currently the most accurate and that no similar publications exist. Therefore, the presented work should be regarded as innovative and is dedicated to close-field UNDEX scenarios, offering a detailed analysis of interactions at short distances. However, the methodologies and findings are versatile and can be extended to far-field scenarios as well.

The numerical simulations in this study were conducted using LS-DYNA, a general-purpose, open engineering software widely recognized for its robust support of arbitrary Lagrangian-Eulerian (ALE) and S-ALE formulations, making it particularly suitable for complex fluid-structure interaction problems such as UNDEX. LS-DYNA provides a comprehensive and practical framework, implementing most standard approaches used in underwater explosion modelling, as outlined in Fig. 3.

However, one method—DYSMAS falls outside the LS-DYNA framework. Developed exclusively for the U.S. Depart-

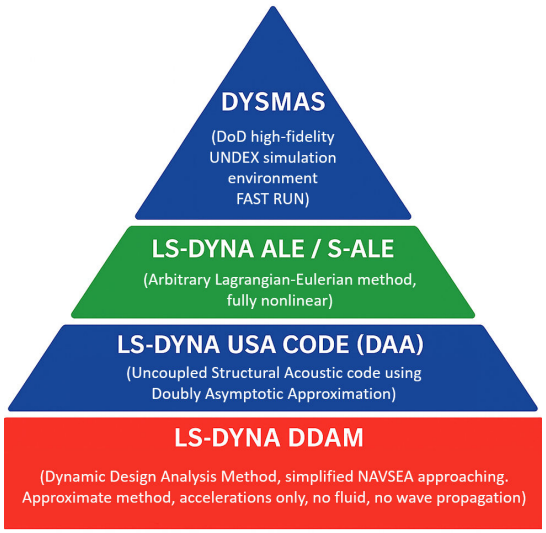


**Fig. 3.** Hierarchy of UNDEX simulation methods and software tools (DoD=Department of Defence (USA) with German cooperation)

ment of Defense, DYSMAS is considered highly accurate but remains restricted, unverifiable, and inaccessible to the public. Therefore, LS-DYNA remains the most practical and accessible solution for academic and civilian UNDEX research.

## 2. CONDITIONS OF THE SIMULATION

In this study, a specific example was chosen to focus on close-field conditions, involving a steel platform with dimensions $12\times10\times5.5$ m, with a thickness of 12 mm subjected to a detonation of a $m = 7$ kg TNT charge placed at a depth of $D = 1.9$ m below the water surface and at a distance of $R = 1.5$ m from the hull. The simulation was carried out as an MMALE case. Materials were defined to accurately reflect the physical conditions, including air within the 'ship', hydrostatic pressure, and the strain rate effect for the steel structure. Figure 4 shows a schematic diagram of the floating structure and the close-in underwater explosion analysis model. Depending on whether a coarse mesh (445 492 elements) or a fine mesh (5 065 736 elements) is used.

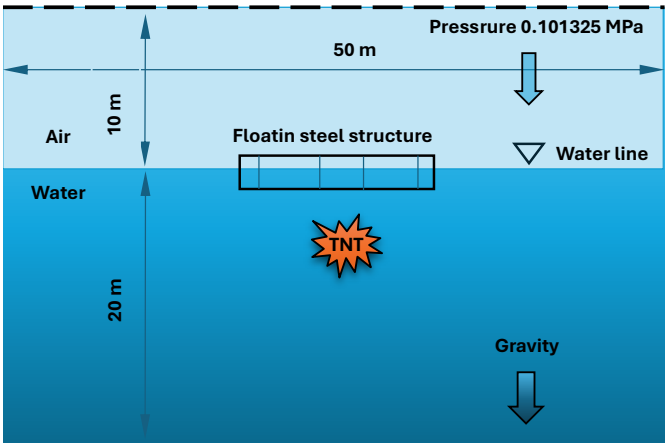


**Fig. 4.** Diagram of the close-in UNDEX simulation

A suitable unit for representing stress is MPa. In LS-DYNA, to display stress in MPa, an appropriate unit system must be chosen. For this reason, the materials and EOS parameters, as referenced in an LS-DYNA keyword file format, are presented as shown in Table 1.

**Table 1**
Unit system used

| Length | Mass | Time | Mass density | Force | Stress |
|---|---|---|---|---|---|
| mm | ton | sec | ton/mm$^3$ | N | N/mm$^2$ = MPa |

The key parameters are presented in the following as fundamental elements of the FEM simulation process.

### Air

In LS-DYNA models, where the physical effects of air play a significant role, the materials `*MAT_NULL` and `*EOS_LINEAR_POLYNOMIAL` are commonly used to represent air. The air above the water follows the ideal gas state equation. The typical input parameters for air at sea level (with an initial pressure of 1 bar) are provided in Table 2.

**Table 2**
Air material parameters for `*MAT_VACUUM` keyword

| Parameter | Value |
|---|---|
| Density, $\rho$, ton/mm$^3$ | $1.2205\cdot10^{-12}$ |
| Pressure cutoff, $p_c$, MPa | 0.0 |

The polynomial equation of state (EOS) is applied, and the pressure is determined using the following equation

$$p = C_0 + C_1\mu + C_2\mu^2 + C_3\mu^3 + (C_4 + C_5\mu + C_6\mu^2)E, \quad (1)$$

where $p$ denotes the pressure, and $C_i$ $(i = 0,1,2,3)$ represents constants with pressure units, meanwhile, $C_i$ $(i = 4,5,6)$ are dimensionless constants. The variable $\mu$ is defined as $\mu = \rho/\rho_0 - 1$, where $\rho/\rho_0$ is the ratio of the current density to the reference density. The parameter $E$ represents the internal energy per unit reference volume, measured in pressure units. The initial relative volume $\upsilon_0$ represents the ratio of the initial volume to the reference volume, typically set to 1.0 for air, ensuring that the material starts in an uncompressed state. This parameter is not directly used in the equations but is listed in Table 3 as part of the material properties, providing a reference value for the initial state.

**Table 3**
Air `*EOS_LINEAR_POLYNOMIA` parameters

| Parameter | Value |
|---|---|
| $C_0 = C_1 = C_2 = C_3 = C_6$ | 0 |
| $C_4$ | 0.4 |
| $C_5$ | 0.4 |
| Initial internal energy, $e_0$, N mm/mm$^3$ | 0.2533125 |
| Initial relative volume, $\upsilon_0$, – | 1.0 |

For air, when $\gamma = c_p/c_\upsilon = 1000$ J/kgK/717 J/kgK $\approx 1.4$ for perfect gases, it defines the specific heat ratio, leading to the relationship $C_4 = C_5 = \gamma - 1 = 1.4 - 1.0 = 0.4$. Under the condition $C_0 = C_1 = C_2 = C_3 = C_6 = 0$, the polynomial EOS simplifies to the ideal gas equation of state

$$p = (\gamma - 1)\frac{\rho}{\rho_0}E = (\gamma - 1)\frac{e_0}{\upsilon_r}, \quad (2)$$

where $E$ has the units of pressure (in the initial state $E = e_0$ and $\upsilon_r = \rho/\rho_0$ is a current relative volume). All parameters of air EOS are presented in Table 3. Initial parameters $\upsilon_0$ and $e_0$ would both consistently define the same initial state for a material.

In the initial state $\rho = \rho_0$, and thus $\mu = 0$ is given in the first step of the computation. Since initial pressure $p_0$ is 0.101325 MPa, the following equation is established $p_0 = C_4 e_0 = 0.101325$ therefore, the initial internal energy $e_0$ is given as $e_0 = \dfrac{0.101325}{0.4} = 0.253313$ MPa = N mm/mm$^3$.

The material parameters and equation of state coefficients for air are presented in Table 4, formatted for direct use in the LS-DYNA solver keyfile. This table contains the necessary input values for defining air properties using the *MAT_NULL and *EOS_LINEAR_POLYNOMIAL models.

**Table 4**

Air material parameters and equation of state coefficients in LS-DYNA keyfile format (ton, mm, s, N, MPa LS-Dyan units)

```
$---+----1----+----2----+----3----+----4----+----5----+----6----+----7----+----8
*MAT_NULL_TITLE
AIR
$#     mid        ro        pc        mu     terod     cerod        ym        pr
           11.2205E-12
$---+----1----+----2----+----3----+----4----+----5----+----6----+----7----+----8
*EOS_LINEAR_POLYNOMIAL_TITLE
EOS AIR
$#   eosid        c0        c1        c2        c3        c4        c5        c6
         1                                              0.4       0.4
$#      e0        v0
 0.2533125       1.0
$---+----1----+----2----+----3----+----4----+----5----+----6----+----7----+----8
```

In many ALE applications involving the interaction of high-density materials, the effects of air are negligible. In such cases, air can be suitably modelled as void using the simple material model *MAT_VACUUM instead of using *MAT_NULL and *EOS_LINEAR_POLYNOMIAL. No input constants are required for *MAT_VACUUM other than the material ID number. Here the vacuum model is automatically generated and appears when a void occurs in the elements.

### WATER

The second stage, and the most important in setting up the simulation, involves accurately modelling the water environment, which plays a critical role in the propagation of shock waves and bubble dynamics. In LS-DYNA, the water domain is represented using an Arbitrary Lagrangian-Eulerian (ALE) formulation to effectively couple the fluid and structural responses. This allows for the simulation of both the initial shock wave and the subsequent gas bubble pulsations triggered by the underwater explosion. The water properties, including density, dynamic viscosity are defined using the *MAT_NULL material model. The typical input parameters for water are provided in Table 5.

**Table 5**

Water material parameters for *MAT_NULL keyword

| Parameter | Value |
|---|---|
| Density, $\rho$, ton/mm$^3$ | $1 \cdot 10^{-9}$ |
| Pressure cut-off, $p_c$, MPa | 0.0 |
| Dynamic viscosity, $\nu$, MPa·s | $1 \cdot 10^{-9}$ |

The equation of state was used for water follows the *EOS_GRUNEISEN model, which accounts for high-pressure conditions, such as those occurring in underwater explosions. The pressure is determined using the Hugoniot relation. The Grüneisen with cubic shock-velocity as a function of particle-velocity $v_s(v_p)$ ($v_s$ – shear wave and $v_p$ – pressure wave), defines pressure for compressed materials as

$$p = \frac{\rho_0 C^2 \mu \left[1 + \left(1 - \frac{\gamma_0}{2}\right)\mu - \frac{a}{2}\mu^2\right]}{\left[1 - (S_1 - 1)\mu - S_2 \frac{\mu^2}{\mu+1} - S_3 \frac{\mu^3}{(\mu+1)^2}\right]} + (\gamma_0 + a\mu)E, \quad \mu > 0 \tag{3}$$

and for expanded materials as

$$p = \rho_0 C^2 \mu + (\gamma_0 + a\mu)E < 0, \quad \mu < 0, \tag{4}$$

where $p$ is the pressure, $C$ is the speed of sound in water. The parameters $S_1$, $S_2$ are derived from the Hugoniot equation, and $\gamma_0$ unit-less Grüneisen gamma, $a$ is the unit-less, first order volume correction to $\gamma_0$ [32], where $\rho$, $\mu$, $E$ represent the same physical concepts as previously defined for air, with $a = 0$. The material constants for the EOS model are provided in Table 6.

**Table 6**

Water *EOS_GRUNEISEN parameters

| Parameter | Value |
|---|---|
| Sound speed in water, $C$, mm/s | 1 452 381.0 |
| $S_1$ | 1.79 |
| $S_2$ | 0 |
| $S_3$ | 0 |
| $\gamma_0$ | 1.65 |
| Initial internal energy, $e_0$, N mm/mm$^3$ | 0.0614091 |
| Initial relative volume, $\upsilon_0$, – | 1.0 |

In this EOS also in the initial state there is $\rho = \rho_0$, and thus $\mu = 0$ is given at the beginning of computation. Since initial pressure $p_0$ is 0.101 325 MPa, the following equation is established $p_0 = \gamma_0 e_0 = 0.101325$ therefore, the initial energy density $e_0$ is given as $e_0 = \dfrac{0.101325}{1.65} = 0.0614091$ MPa $\equiv$ N/mm$^2$ $\equiv$ N mm/mm$^3$, where $p_0$ represents the reference pressure term derived from the Hugoniot relation in the *EOS_GRUNEISEN model, linking the initial specific energy $e_0$ and the coefficient $S_1$.

The difference in volumetric internal energy $e_0$ (between air 0.253313 MPa and water 0.061409 MPa) arises from the compressibility of these media. In gases, pressure waves propagate at lower speeds due to their high compressibility, which results in a higher volumetric energy value. In contrast, liquids like water are nearly incompressible, causing pressure waves to travel much faster and leading to a lower volumetric internal energy for the same energy input. This difference is crucial in underwater explosion simulations, where the transmission of shock waves depends on the medium bulk modulus and equation of state (EOS).

The relationship between volumetric internal energy and pressure differs significantly between water and air due to their compressibility. In water, pressure increases rapidly with energy because of its high bulk modulus ($K \approx 2200$ MPa), meaning small energy changes result in significant pressure variations. In air, pressure rises more gradually, as it is highly compressible ($K \approx 0.1$ MPa), allowing more energy storage before a notable pressure increase occurs. This distinction is crucial in shock wave propagation (pressure waves in water travel faster and with greater intensity), impacting underwater explosion effects, whereas in air, energy disperses more gradually, leading to extended pressure wave development over time.

The Grüneisen equation of state (EOS) typically assigns a low adiabatic index $\gamma_0$ for liquids, around $\gamma_0 \approx 0.28$. This re-

flects the near-incompressibility of water under normal conditions. However, in underwater explosion (UNDEX) scenarios, extreme pressures and shock wave dynamics require a higher value $\gamma_0 \approx 1.65$. This adjustment accounts for the compressibility effects at high pressures, cavitation phenomena, and the specific propagation characteristics of shock waves in water [1]. Other studies have used lower values (e.g., $\gamma_0 = 0.11$ with TNT charge 0.05 kg [26]), but for high-pressure shock conditions, a higher $\gamma_0$ is required.

Since water is nearly incompressible under normal conditions, a standard equation of state would fail to correctly describe its behaviour in extreme pressure environments. The `*EOS_GRUNEISEN` formulation compensates for this by incorporating the reference pressure term $p_0$, which accounts for the initial energy density $e_0$, and by including empirical parameters that improve the representation of shock wave propagation. This is especially important in ALE simulations, where high-density materials require explicit modelling to capture fluid-structure interactions. The `*EOS_GRUNEISEN` model ensures that realistic hydrostatic behaviour is preserved, particularly in the transmission of shock waves and bubble pulsations.

The material parameters and equation of state coefficients for water are presented in Table 7, formatted for direct use in the LS-DYNA solver key file.

**Table 7**

Water material parameters and equation of state coefficients in LS-DYNA keyfile format (ton, mm, s, N, MPa LS-Dyan units)

```
$---+----1----+----2----+----3----+----4----+----5----+----6----+----7----+----8
*MAT_NULL_TITLE
WATER
$#     mid        ro        pc        mu      terod      cerod        ym        pr
         21.00000E-9          1.00000E-9
$---+----1----+----2----+----3----+----4----+----5----+----6----+----7----+----8
*EOS_GRUNEISEN_TITLE
EOS WATER
$#   eosid         c        s1        s2        s3    gamma0         a        e0
         2   1452381      1.79                          1.65            0.0614091
$#      v0    unused      lcid
       1.0
$---+----1----+----2----+----3----+----4----+----5----+----6----+----7----+----8
```

### TNT

The TNT explosive used in the simulation was modelled using the `*MAT_HIGH_EXPLOSIVE_BURN` material model, which parameters were presented in Table 8.

**Table 8**

TNT material parameters for `*MAT_HIGH_EXPLOSIVE_BURN`

| Parameter | Value |
|---|---|
| Density, $\rho$, ton/mm$^3$ | $1.63 \cdot 10^{-9}$ |
| Detonation velocity, $D$, mm/s | $6930 \cdot 10^3$ |
| Chapman-Jouguet pressure, $p_{CJ}$, MPa | 21 000.0 |

This formulation, combined with the Jones-Wilkins-Lee (JWL) equation of state `*EOS_JWL`, allows for accurate representation of the detonation process and the subsequent energy release from the explosive. The parameters defining TNT include its density, detonation velocity, and Chapman-Jouguet pressure, ensuring an accurate characterization of the rapid expansion of detonation gases.

The JWL equation of state is used to describe the pressure of detonation products as

$$P = A\left(1 - \frac{\omega}{R_1 V}\right)e^{-R_1 V} + B\left(1 - \frac{\omega}{R_2 V}\right)e^{-R_2 V} + \frac{\omega E}{V}, \qquad (5)$$

where $A$, $B$, $R_1$, $R_2$, and $\omega$ are empirical constants, $V$ is the relative volume, and $E$ is the internal energy per unit initial volume. The parameter $\omega$ represents the adiabatic expansion coefficient of detonation gases, controlling the contribution of internal energy to pressure. A higher value of $\omega$ indicates a more compressible gas where internal energy plays a greater role, while a lower value suggests that pressure is primarily governed by gas expansion. These parameters allow the model to capture both the initial shock wave and the subsequent expansion and pulsation of the detonation gases and were presented in Table 9.

**Table 9**

TNT equation of state parameters for `*EOS_JWL`

| Parameter | Value |
|---|---|
| $A$, MPa | 371 213 |
| $B$, MPa | 3230.6 |
| $R_1$ | 4.15 |
| $R_2$ | 0.95 |
| $\omega$ | 0.3 |
| Initial internal energy, $e_0$, Nmm/mm$^3$ | 6000 |
| Initial relative volume, $\upsilon_0$, – | 1.0 |

Key files parameters defining TNT include its density, detonation velocity, and Chapman-Jouguet pressure. The `JWL` equation of state parameters were set as below in Table 10, ensuring an accurate representation of the rapid energy release and expansion of explosion-generated gases.

**Table 10**

TNT material parameters and equation of state coefficients in LS-DYNA keyfile format (ton, mm, s, N, MPa LS-Dyan units)

```
$---+----1----+----2----+----3----+----4----+----5----+----6----+----7----+----8
*MAT_HIGH_EXPLOSIVE_BURN_TITLE
TNT
$#     mid        ro         d       pcj      beta         k         g      sigy
         3  1.630E-9   6930000   21000.0
$---+----1----+----2----+----3----+----4----+----5----+----6----+----7----+----8
*EOS_JWL_TITLE
EOS TNT
$#   eosid         a         b        r1        r2      omeg        e0        vo
         3  371213.0    3230.6      4.15      0.95       0.3    6000.0       1.0
$---+----1----+----2----+----3----+----4----+----5----+----6----+----7----+----8
```

The input values for TNT explosives have been referenced in published papers containing both experimental and computational studies. This setup allows the simulation to replicate both the initial blast wave and the subsequent gas bubble pulsations, which are critical for analyzing the structural response of the floating platform. The detonation model was validated against established UNDEX benchmarks to provide reliable insights into the interaction of the shock wave with the surrounding medium.

This configuration enables the simulation to replicate both the initial shock wave and the subsequent gas bubble pulsations

(Fig. 5), which are critical for analyzing the structural response of the floating platform. The detonation model was calibrated to ensure compatibility with the scale and boundary conditions of the UNDEX scenario, providing reliable insights into the shock wave propagation and structural interactions.

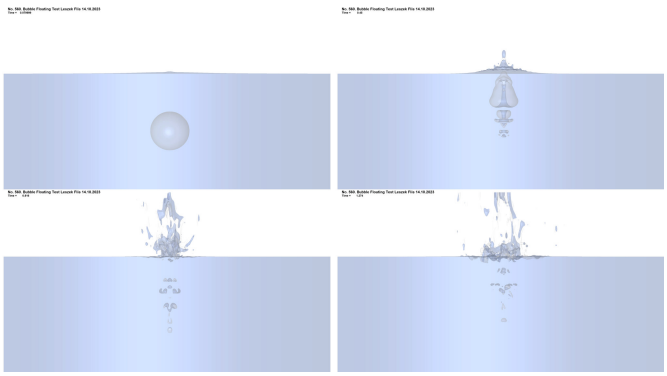

**Fig. 5.** Simulation of a pure underwater explosion, illustrating bubble pulsation

The presented parameters, refined through multiple iterations, produced a realistic simulation of an underwater explosion, effectively replicating bubble pulsation and cavitation. Further experimental validation is planned to improve confidence in these findings.

## STEEL

Further work on the UNDEX simulation requires material modelling, which is as critical as the previously discussed simulation parameters. The material of the floating structure was set as stainless steel, and the structure was modelled by considering the strain rate effect in the standard elastoplastic model. Due to the necessity of accounting for strain rate effects in the steel material, AISI 304 (also known 1.4301), a well-documented stainless steel [33], was selected for this case.

The author has resolved the challenges of modelling steel behavior by employing the `*MAT_JOHNSON_COOK` material model. To determine its parameters, a split Hopkinson pressure bar setup was developed and user material subroutine `*MAT_USER_DEFINED_MATERIAL_MODELS`, enabling accurate characterization of strain rate sensitivity. However, further comparative studies are planned to evaluate the advantages, drawbacks, and sometimes the unjustified complexity of using the advanced model over simpler alternatives. For this paper, AISI 304 was used to ensure that the results remain accurate and reliable within the stress range of interest, leveraging the steel comprehensive documentation. The parameters for the steel material model were defined in Table 11. The parameters for the steel material model formatted directly for the LS-DYNA solver keyfile were presented in Table 12.

Figure 6 illustrates the strain rate effect curve for used material, modelled using the Cowper & Symonds formulation. This curve highlights the relationship between strain rate and the scaling factor applied to the yield stress. As the strain rate increases, the scaling factor grows significantly, demonstrating the material enhanced resistance to deformation under dynamic loading conditions.

The inclusion of Fig. 7 serves to visualize the impact of the Cowper & Symonds parameters ($C$ and $P$) on the material response. It provides a clear reference for understanding how strain rate sensitivity is captured in the simulation, espe-

**Table 11**
AISI 304 material parameters for
`*MAT_PIECEWISE_LINEAR_PLASTICITY`

| Parameter | Value |
|---|---|
| Density, $\rho$, tons/mmm$^3$ | $7.930 \cdot 10^{-9}$ |
| Young's modulus, $E$, MPa | $1.95 \cdot 10^5$ |
| Poisson's ratio, $\nu$ | 0.3 |
| Yield stress, $\sigma_y$, MPa | 320 |
| Failure strain, $\varepsilon_{\text{fail}}$ | 0.7 |
| Strain rate coefficient, $C$ | 4000 |
| Strain rate exponent, $P$ | 4.0 |

**Table 12**
Material card definition for AISI 304 used incorporating strain rate effects with Cowper & Symonds parameters

```
$---+----1----+----2----+----3----+----4----+----5----+----6----+----7----+----8
*MAT_PIECEWISE_LINEAR_PLASTICITY
$# SUS304 include strain rate effects
$#      mid        ro         e        pr      sigy      etan      fail      tdel
         101  7.930E-9  195000.0       0.3     320.0                 0.70    1.0E-8
$#        c         p      lcss      lcsr        vp
   40000.0       4.0       304                -1.0
$#     eps1      eps2      eps3      eps4      eps5      eps6      eps7      eps8

$#      es1       es2       es3       es4       es5       es6       es7       es8

$---+----1----+----2----+----3----+----4----+----5----+----6----+----7----+----8
*DEFINE_CURVE
$#     lcid      sidr       sfa       sfo      offa      offo    dattyp     lcint
         304                1.0       1.0
$#               a1                   o1
             0.000000          320.000000
             0.020000          386.000000
             0.050000          453.500000
             0.100000          553.500000
             0.300000          933.500000
             0.500000         1283.500000
             0.600000         1393.500000
             0.700000         1493.500000
             0.800000         1568.500000
             0.900000         1628.500000
             1.000000         1668.500000
             1.200000         1720.500000
             1.400000         1760.500000
             1.600000         1790.500000
             1.800000         1812.500000
             2.000000         1828.500000
             2.500000         1851.000000
             3.000000         1861.000000
$---+----1----+----2----+----3----+----4----+----5----+----6----+----7----+----8
```

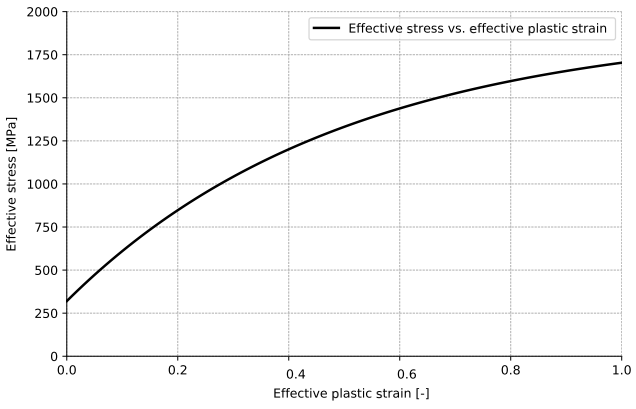


**Fig. 6.** Effective stress vs. effective plastic strain curve for stainless steel

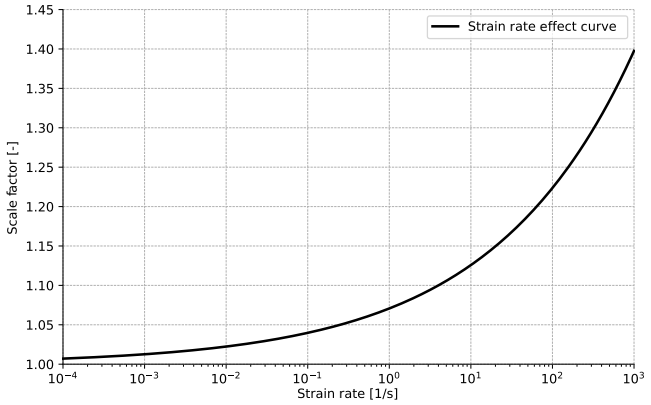


**Fig. 7.** Strain rate effect curve of stainless steel

cially under high-speed deformation scenarios typical of underwater explosion (UNDEX) phenomena. This foundational analysis is crucial for validating the applied material model and serves as a baseline for future studies incorporating more advanced constitutive and failure models. The Cowper & Symonds model is widely used in simulations to account for strain rate effects in materials due to its computational efficiency. While the keyfile explicitly defines the material model as `*MAT_PIECEWISE_LINEAR_PLASTICITY`, the strain rate effects are implicitly incorporated by the solver using the Cowper & Symonds formulation

$$\sigma_y\left(\varepsilon^P_{\text{eff}}, \dot{\varepsilon}^P_{\text{eff}}\right) = \sigma^s_y\left(\varepsilon^P_{\text{eff}}\right) + \text{SIGY} \times \left(\frac{\dot{\varepsilon}^P_{\text{eff}}}{C}^{\frac{1}{P}}\right), \tag{6}$$

where:

$\sigma_y$ – yield stress,
$\sigma^s_y$ – quasi-static yield stress,
SIGY – scaling factor,
$\varepsilon^P_{\text{eff}}$ – effective plastic strain,
$\dot{\varepsilon}^P_{\text{eff}}$ – effective plastic strain rate,
$C$ – strain rate coefficient (Cowper & Symonds parameter),
$P$ – strain rate exponent (Cowper & Symonds parameter).

If the deformation of the floating structure is too small compared to the experimental result, the strain rate effect may be too large. Conversely, if the deformation is too large compared to the experimental result, the strain rate effect may be too small. Therefore, it is recommended to adjust the values of $C$ and $P$ and then verify the results.

The `MAT_015` (Johnson-Cook model) is widely recognized and highly popular as a constitutive material model. However, its use requires specialized equipment for accurately determining the model parameters, which are often taken directly from the literature without proper interpretation—a common mistake. One of the key features of the Johnson-Cook model is its incorporation of temperature effects, yet this aspect is frequently neglected due to the lack of advanced experimental setups for parameter determination under varying temperature conditions. As a result, the model is often reduced to accounting primarily for strain rate effects, producing results similar to those obtained with simpler material models.

On the other hand, `MAT_024` provides a reliable representation of the deformation behaviour of the entire floating structure while being straightforward to understand and implement. This makes `MAT_024` a practical choice for applications where the additional complexity of `MAT_015` may not offer significant advantages, particularly when temperature-dependent effects are not rigorously included.

The presented material parameters effectively capture the plastic deformation and buckling phenomena, as illustrated in Fig. 8. These results demonstrate the model's capability to simulate structural response under UNDEX conditions, including areas of plasticity and localized instability. While the damage parameter included in the model is simplified at this stage, this initial approach focused on normalizing known baseline parameters. This normalization serves as a reference for future studies employing more advanced constitutive and failure model `*MAT_PIECEWISE_LINEAR_PLASTICITY` that provides multiple ways to define strain rate effect.

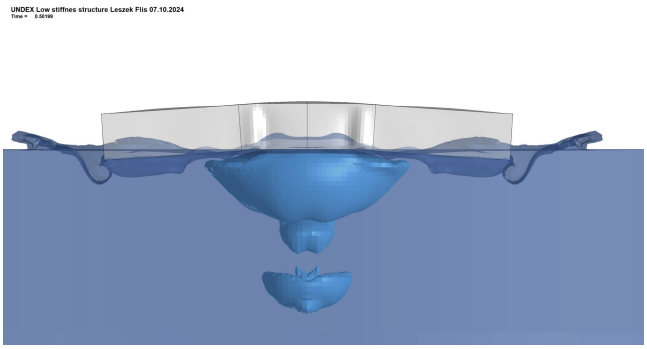


**Fig. 8.** Buckling of a structure as a result of UNDEX pulsation

The purpose of this initial study was to establish a foundation for comparing the effectiveness and limitations of different material modelling approaches. Future work will incorporate more complex damage mechanisms, allowing for a deeper evaluation of model accuracy and potential sources of error. The validation of these simulations will pose a significant challenge due to the specific nature of underwater explosion phenomena, which are inherently difficult to replicate experimentally. However, a series of publications is planned, using this study as a reference point, to progressively refine and validate the numerical models through experiments. These experiments, while demanding, will provide crucial insights into the behaviour of materials under extreme dynamic loading conditions.

Since gravity acts on the water region, the hydrostatic pressure is distributed according to the water depth. The behavior of explosion–generated gas bubbles caused by an underwater explosion is influenced by water pressure. Therefore, it is essential to introduce the water pressure distribution based on the water depth as the initial condition of the analytical model.

The remaining settings, apart from those mentioned, are based on standard ALE commands in LS-DYNA. However, their proper application requires careful attention and a solid understanding of the documentation to ensure accurate completion of the simulation.

### BOUNDARY AND FLUID-STRUCTURE INTERACTION

Considering that the experiment is implemented in natural water, the *INITIAL_ALE_HYDROSTATIC keywords are used to initialize the atmospheric pressure and hydrostatic gradient pressure under the far-field environmental boundary and the full-field gravity.

In the present simulation, the interaction between water (the fluid medium, represented using an Eulerian mesh) and the structure (modelled in the Lagrangian framework) was captured using an ALE–Lagrange coupling approach, implemented via the *CONSTRAINED_LAGRANGE_IN_SOLID keyword. This method enables accurate transmission of pressure from the fluid to the structure, while accounting for structural deformation and potential material erosion.

Non-reflecting boundary condition does not define the flow rate at the boundary surface. Therefore, when non-reflecting boundary condition is applied to the bottom or sides of the analysis model, the gravitational acceleration will cause the water in the analysis model to flow out from the boundary surface to the outside area. That is why non-reflecting boundary condition cannot be used for underwater explosion analyses.

Instead, rigid boundary condition must be defined for the sides and bottom of the analysis model. The rigid boundary condition is expressed by setting the boundary SPC condition or the ALE essential boundary condition, which are flow rate regulation conditions.

Please note that the nonreflecting boundary condition (boundary nonreflecting) and a flow rate regulation condition (boundary SPC or ALE essential boundary) cannot be used simultaneously for the same boundary surface.

In order to reduce the impact on the analysis results due to the rigid boundary truncating the area that continues to infinity, we need to create a model that secures the area of the analysis model sufficiently large for the area where the impact of the explosion is large so that the influence of the boundary surface does not significantly affect the analysis evaluation zone. It has been confirmed that, when approximating a free field in an underwater explosion analysis, the water domain should extend at least $6 \times r_{\text{bubble}}$ in all directions.

In the future work, the simulation will be conducted using the new S-ALE solver, which is more efficient, especially in fluid-structure interaction problems involving large deformations and gravity. One of the key advantages of the S-ALE formulation is the improved handling of boundary conditions. In traditional ALE models, applying BOUNDARY_NON_REFLECTING on the bottom face in the presence of gravity often led to unphysical fluid outflow–the water would "fall through" the mesh due to the absence of proper mass constraints, causing spurious pressure drops and reflections. In contrast, the S-ALE solver provides a more robust and user-friendly approach via the *BOUNDARY_SALE_MESH_FACE card, which allows precise definition of boundary behaviour. For instance, setting the bottom face as NOFLOW prevents downward fluid escape, maintaining hydrostatic balance. At the same time, NONREFL boundaries can be applied to the lateral and upper faces to minimize artificial wave reflections. This results in significantly improved stability and realism in UNDEX simulations, especially when modelling free-surface interactions under gravity.

### DAMPING

Damping has long been a critical aspect of ship shock modelling and simulation. Although several published [34, 35] and unpublished [36–38] studies have investigated damping mechanisms, it remains a challenging parameter to define accurately. Recent findings [39, 40] have contributed to the development of improved damping models, particularly in the context of numerical simulations using LS-DYNA.

A commonly used approach is Rayleigh damping, defined as:

$$[\mathbf{C}] = \alpha[\mathbf{M}] + \beta[\mathbf{K}], \tag{7}$$

where $[\mathbf{C}]$ is the damping matrix, $[\mathbf{M}]$ the mass matrix, and $[\mathbf{K}]$ the stiffness matrix. The coefficients $\alpha$ and $\beta$ are typically selected to produce a modal damping ratio in the range of 2% to 5%, which reflects energy dissipation mechanisms such as welded joints, internal friction, and structural fittings in ship hulls. In the present study, representative values of $\alpha = 0.004$ and $\beta = 0.15$ were applied, following the recommendations from [39].

While damping has minimal effect on the peak structural response during the initial shock wave propagation, it can significantly influence residual vibrations and energy dissipation in later stages of the transient response. In this study, damping was included for completeness within the general modelling framework; however, its influence was not the focus of analysis and will be addressed in future work.

Due to the short duration of the considered shock event, damping effects are assumed to be negligible in terms of peak structural response. Indeed, several studies [21, 41] deliberately omit damping to preserve the accuracy of peak pressure and displacement predictions. Furthermore, in UNDEX simulations, the shock wave and cavitation effects are primarily governed by the equation of state and artificial viscosity, which provide sufficient numerical dissipation for capturing high-frequency phenomena.

Nevertheless, the author recognizes the importance of damping in structural dynamic analyses and plans to conduct dedicated studies on its influence on the results of underwater explosion simulations in future work.

## 3. DISCUSSION OF SIMULATION RESULTS

In experiments involving close-in underwater explosions near a floating structure (opposite to far–field), it has been challenging to clearly understand the detailed behavior of the explosion-generated gas bubbles due to the difficulties associated with visualizing these events [23]. For that reason, FEM simulation is a good solution to deeply study a phenomenon of the issue.

This is because the floating structure has already sustained significant damage from the initial shock wave of the close-in explosion. Consequently, it is necessary to track the physical

phenomena over an extended period to accurately evaluate the deformation and damage of the floating structure in a close-in underwater explosion, which complicates the analysis.

Moreover, the limited quantity of explosives permissible in laboratory settings poses significant challenges for conducting experiments that could result in substantial damage to floating structures. Consequently, there is an increasing demand for numerical analysis to explore the interplay between various factors and scenarios, such as the type and amount of explosive, water depth, standoff distance (i.e., the distance from the structure), the pulsation behavior of explosion-induced gas bubbles, and the deformation and damage to floating structures during close-in underwater explosions. These investigations are crucial for gaining insights into the problem before conducting real-world trials.

A noticeable discrepancy exists between the high-pressure values depicted in Fig. 9 (ranging from approximately −255 MPa to 290 MPa) and the lower peak pressure at the time $t = 0.015$ s recorded by FSI trackers, which reaches only around 17 MPa during the initial shock wave phase. This difference can be attributed to the inherent characteristics of the FSI method and the numerical representation of shock wave interactions with the plate.

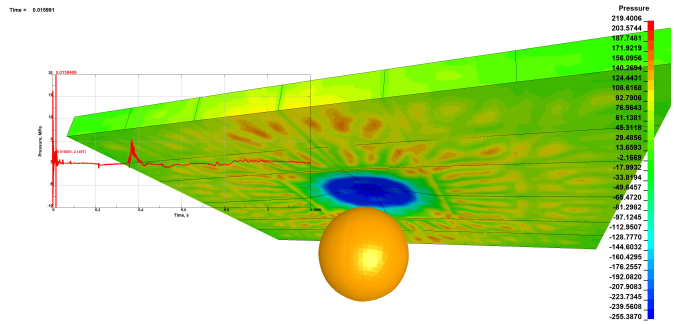


**Fig. 9.** Pressure distribution on the floating structure at time $t = 0.016$ ms after detonation (unit MPa)

High pressures in Fig. 9 reflect localized shockwave effects and structural deformation, captured by the finite element mesh in small regions. The effects of these localized pressures lead to stress distributions across the plate, which result in stress distributions, as shown in Fig. 10, where von Mises stresses highlight regions of significant deformation and structural response.

Conversely, the FSI tracker measures the effective fluid-structure interaction pressure averaged over a predefined area. This averaging inherently smooths out the localized peaks, reflecting the effective load transmitted to the structure rather than the local extremes. Additionally, the dynamic response of the plate redistributes the load over time, reducing the instantaneous peak pressure captured by the FSI tracker.

This distinction highlights the importance of interpreting FSI results in the context of global structural behavior, while localized stresses and pressures should be analyzed separately for understanding specific material or design vulnerabilities. Together, these observations provide complementary insights into

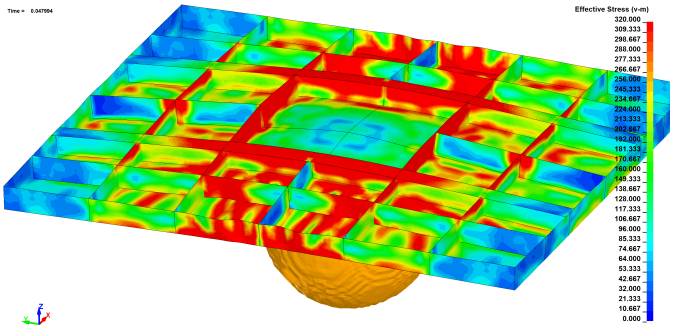


**Fig. 10.** Effective stress distribution (von Mises) on the floating structure at time $t = 0.047$ ms after a close–in UNDEX (unit MPa)

the complex interaction dynamics during an underwater explosion.

A far-field UNDEX is relatively well-described in the literature [17] and the characteristic features of pressure wave propagation, such as the smooth decay of peak pressure and the extended duration of the impulse, are well understood and widely documented. This stands in contrast to close-field UNDEX, where these phenomena are less well-defined. For this reason, it is desirable to compare the results with both experimental data and empirical equations.

In this paper, the FEM UNDEX results are compared with theoretical predictions to assess whether the simulation yields the expected outcomes. The results of the UNDEX simulation were analyzed and compared with theoretical predictions for maximum pressure, bubble radius, and oscillation times. The empirical equations, derived from [42], determine the maximum pressure ($p_{\max}$), the maximum radius of the gas bubble ($r_{\text{bubble}}$), the period of bubble oscillation ($T$). However, it should be noted that these equations are not optimally applicable in the immediate vicinity of the explosive charge, due to their reliance on idealized conditions, which often lead to overestimated pressure values in such scenarios [42, 43].

The entire simulation and structural response analysis were conducted under consistent conditions, with the explosive charge positioned at a depth of 1.9 m and at a distance of 1.5 m from the bottom of the hull. This configuration was chosen to simulate a near explosion, where the gas bubble remains in significant contact with the structure during its expansion and collapse phases.

For a more precise assessment of the explosion dynamics in water, minimizing the effects of surface reflections and structural interactions, and for comparison of the simulation results with analytical predictions, a detailed analysis was performed with the charge placed at a depth of 3.95 m. This configuration ensured that the entire gas bubble remained fully submerged during the initial expansion phase, allowing for an accurate examination of the bubble behaviour without interference from the water surface or nearby structures.

A typical pressure profile for a far-field UNDEX compared to close-field UNDEX, given by (8) is shown in Fig. 11, is ten times higher, and the values are consistent with expectations.

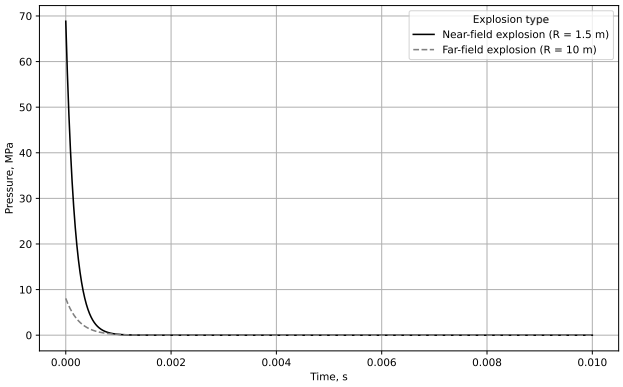


**Fig. 11.** Comparison of pressure for near-field and far-field UNDEX Explosions for the presented case (7 kg TNT)

$$p(t) = p_{\max} \cdot e^{-t/\theta} = 52.12 \left( \frac{\sqrt[3]{m}}{R} \right)^{1.18} \cdot e^{-t/\theta}, \quad \text{MPa}, \tag{8}$$

where:
$p(t)$ – pressure at time $t$, s,
$m$ – explosive charge mass, kg,
$R$ – standoff distance from a charge, m,
$\theta$ – time constant, $0.000092 \cdot \sqrt[3]{m} \left( \frac{\sqrt[3]{m}}{R} \right)^{-0.185}$, s.

$$R_{b_{\max}} = 3.383 \cdot \frac{\sqrt[3]{m}}{(H+10.1)^{1/3}}, \quad \text{m}, \tag{9}$$

where:
$R_{b_{\max}}$ – max. radius of the gas bubble, m,
$m$ – explosive charge mass, kg,
$H$ – charge depth, m,
$10.1 \approx \frac{p_0}{\rho_{sw} g} \approx \frac{101325}{1025 \cdot 9.81}$ – seawater head, m; 10.3 for fresh water.

$$T = 2.064 \cdot \frac{\sqrt[3]{m}}{(H+10.3)^{5/6}}, \quad \text{s}, \tag{10}$$

where:
$T$ – bubble oscillation period, s,
$m$ – explosive charge mass, kg,
$H$ – charge depth, m.

Table 13 summarizes the theoretical (given by (8), (9) and (10)) and simulation results, along with the calculated relative errors. The comparison shows that the maximum pressure, bubble diameter, and full oscillation period are closely aligned between theoretical predictions and simulation results. The relative errors are below 8.5% for pressure, 1.69% for bubble diameter, and only 3.57% for the full oscillation period, demonstrating agreement.

**Table 13**
Comparison of theoretical and simulation results for UNDEX analysis

| Parameter | Theoretical value | Simulation value | Relative error (%) |
|---|---|---|---|
| Maximum pressure, $p_{\max}$, MPa | 69.44 | 63.50 | 8.5 |
| Bubble diameter, $2 \cdot R_{b_{\max}}$, m | 5.34 | 5.25 | 1.69 |
| Full oscillation period, $T$, s | 0.56 | 0.54 | 3.57 |

The relative error for maximum pressure (8.5%) can be attributed to the inherent limitations of theoretical equations, such as those by Cole, which tend to overestimate results by approximately 10%. These equations assume linear acoustic propagation, which is most accurate at distances between 10 and 100 charge radii. At closer ranges, such as in this case, nonlinear effects and complex shock wave interactions result in discrepancies.

The bubble diameter shows exceptional agreement, with a relative error of only 1.69%. This high level of accuracy highlights the robustness of the numerical model and its ability to capture the complex physical phenomena associated with underwater explosions, even under near-surface conditions.

Figure 12 illustrates key results, including pressure, acceleration, and velocity during an underwater explosion. The pressure graph 12a shows a sharp peak from the shock wave, followed by diminishing oscillations caused by gas bubble pulsations.

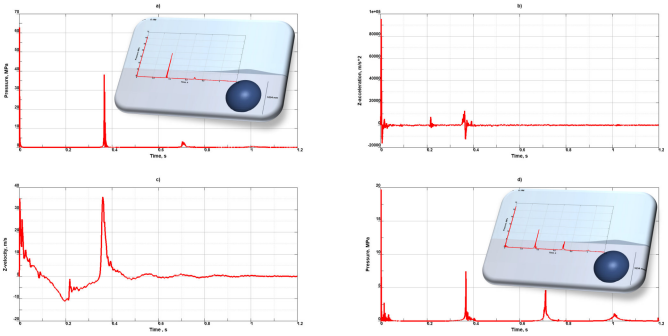

**Fig. 12.** Tracking UNDEX results: (a) maximum pressure $p_{\max}$, (b) acceleration, (c) velocity, (d) pressure measure closer to the surface at distance 1.5 m

This behaviour is consistent with theoretical predictions, where the maximum pressure is observed during the shock wave. Figure 12b shows the acceleration response, with a pronounced peak at the shock wave impact and subsequent oscillations that align with bubble pulsations. Similarly, Fig. 12c indicates velocity changes, characterized by an initial rapid spike followed by oscillations driven by the expanding and collapsing gas bubble. Finally, Fig. 12d demonstrates the pressure, where the maximum values decrease closer to the surface due to energy dissipation, while oscillatory effects become more pronounced. These trends are consistent with expected physical phenomena.

The oscillatory behaviour of the floating structure, resulting from both the initial shock wave and subsequent gas bubble pulsations, was clearly observed and tracked over time. As shown in Fig. 12b and Fig. 12c, acceleration and velocity responses of the structure exhibit a high-frequency spike during the initial impact, followed by damped oscillations aligned with the pulsation phases of the explosion-generated gas bubble. These induced vibrations are consistent with whipping effects and are indicative of the dynamic structural response caused by close–in UNDEX events.

Figure 13a illustrates the bubble oscillation dynamics resulting from the underwater explosion. The simulation results demonstrate that the amplitude of the second pulsation is approximately 70% of the first, while the third pulsation reaches about 50% of the initial amplitude. This trend is clearly visible in Fig. 13, where the reduction in amplitude aligns well with theoretical expectations.

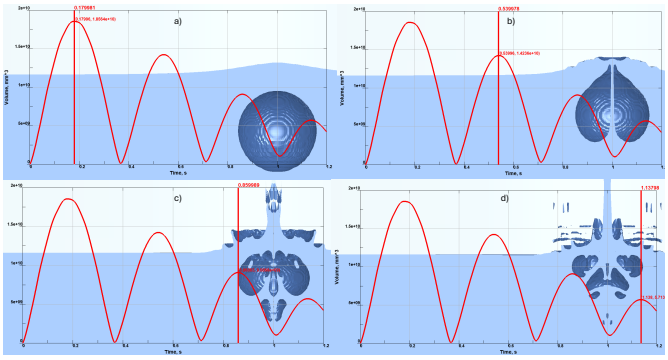

**Fig. 13.** Tracking UNDEX results: (a) first pulsation at $t \approx 0.179$ s, (b) second pulsation at $t \approx 0.54$ s, (c) third pulsation at $t \approx 0.85$ s, (d) subsequent pulsations showing decreasing amplitude and energy dissipation $t \approx 1.13$ s

The consistent decrease in pulsation amplitude reflects the progressive dissipation of energy into the surrounding water and the interaction effects with the free surface. As shown in Fig. 13b, the oscillation of the bubble volume follows the same pattern, confirming the energy loss and its redistribution in the surrounding medium. Furthermore, the observed behavior is in agreement with theoretical models that predict diminishing amplitudes while maintaining approximately constant pulsation periods. The results presented in Fig. 13 provide further evidence supporting the validity and accuracy of the finite element simulation. Theoretical predictions align with simulations, validating the numerical model ability to capture bubble dynamics.

Figure 14 shows the pressure distribution in water at different moments of the analysis (0.003 s, 0.36 s, 0.71 s, and 1.0 s). The figure highlights the propagation of the shock wave, the formation and collapse of the gas bubble, and the resulting pressure gradients in the surrounding water. The highest pressures are observed near the centre of the explosion, diminishing as the shock wave dissipates. These pressure distributions are not only indicative of the energy release and dissipation process but also closely correlate with the cavitation phenomena, as regions of low pressure shown in this figure coincide with areas of cavitation depicted in Fig. 15.

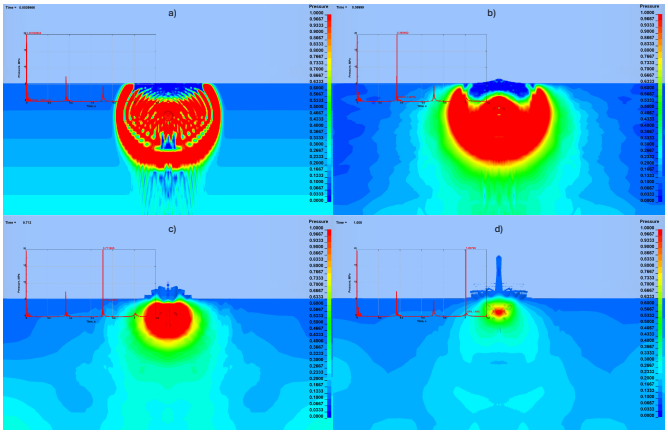

**Fig. 14.** Pressure distribution in the water (unit MPa)

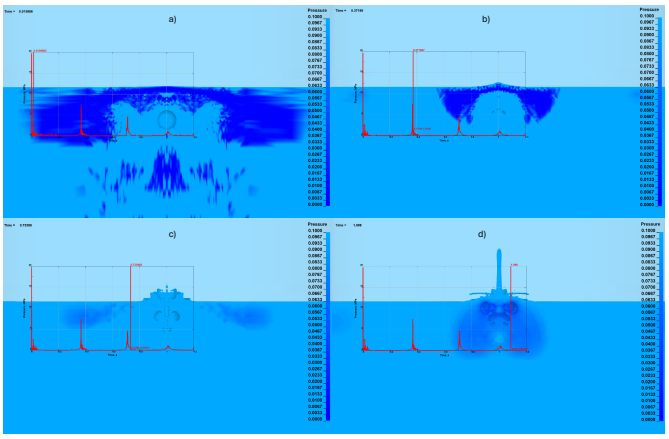

**Fig. 15.** Visualization of cavitation regions (unit MPa)

Figure 15 highlights areas where the water pressure drops to approximately 0 MPa, leading to cavitation and the formation of vapour bubbles. These regions are indicative of the extreme pressure gradients caused by the shock wave and subsequent oscillations of the gas bubble. The extent of cavitation evolves over time, correlating with the pulsating dynamics of the explosion.

The relationship between the pressure gradients (Fig. 14) and the cavitation zones (Fig. 15) underscores the accuracy of the simulation in capturing both macroscopic shock wave propagation and microscopic phenomena such as cavitation.

The simulation results show that part of the pressure wave is reflected from both the free surface and the floating structure itself, influencing subsequent load phases. These reflections contributed to secondary pressure peaks observed in the fluid domain and structural response, visible in the pressure distribution maps (Fig. 15) and in the oscillatory tail of acceleration and pressure plots (Fig. 12). The constructive and destructive interference of incident and reflected waves significantly altered the dynamic pressure field, confirming the importance of capturing wave reflections in near-field UNDEX modelling.

The simulation explicitly captured regions of low pressure approaching 0 MPa (Fig. 15), indicative of cavitation and localized vapour formation. These zones reflect areas where the pressure dropped significantly below the ambient hydrostatic level due to rapid bubble expansion and collapse, effectively simulating vacuum-like conditions. While a full vapour-phase model was not included, the pressure fields and cavitation visualizations confirm the model capability to replicate pressure rarefaction and transient vacuum effects, which are critical in the context of high-intensity bubble dynamics.

At large distances, both the shock wave and gas bubble are weak, causing little to no damage. At very short distances, the shock wave is strong, but the gas bubble collapses prematurely

if too close to the water surface, dispersing its energy as foam and limiting destructive potential.

Maximum damage occurs at an optimal distance—neither too close nor too far—where a stable gas bubble can fully develop and release energy through pulsations and jets acting on the structure.

In deep water, the gas bubble destructive potential may exceed that of the shock wave. Ignoring this effect risks underestimating the weapon power. For maximum efficiency, full use of bubble effects is essential.

## 4. FUTURE WORK

Future studies will build upon and validate the present work using available experimental results (Fig. 16) [26]. and integrating numerical and empirical approaches to enhance the reliability and applicability of underwater explosion models. This study serves as the foundation for a series of publications, aiming to introduce the reader to the theoretical framework necessary for accurately replicating numerical simulations. While experimental results are available for comparison, the primary objective at this stage is to present the extensive numerical research conducted over the years, which constitutes a significant achievement within the existing body of literature.

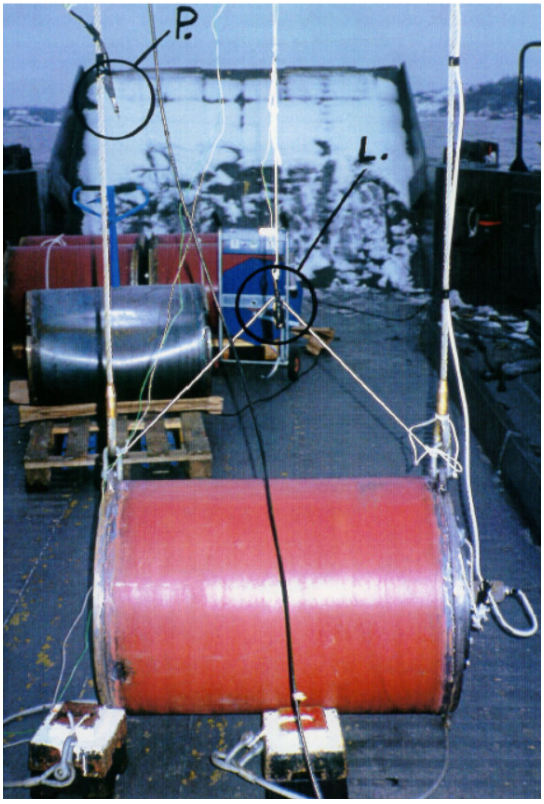


**Fig. 16.** Barrel before explosion test with wires and weights. The pressure gauge is marked with a P and the charge with an L [26]

The advancements achieved in numerical modelling and simulation of underwater open new possibilities for future research, aimed at addressing increasingly complex scenarios and challenges. Each figure presented outlines distinct directions for further development, underscoring the versatility and potential of the applied methods.

Figure 17 highlights simulations of submerged structures, such as submarines, with a particular emphasis on their interaction with the seabed. Future research in this area will focus on refining algorithms to better account for seabed effects and their influence on shock wave propagation. This will be crucial in developing guidelines for designing and evaluating the resilience of underwater vehicles and infrastructure operating in close proximity to the seabed.

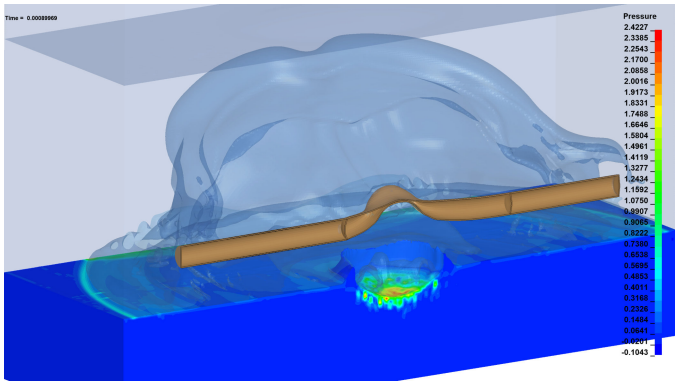


**Fig. 17.** Simulation of submerged structures subjected to underwater explosions, emphasizing the interaction of shock waves with the seabed and its effect on structural deformation (unit MPa)

Figure 18 illustrates simulations of pipeline systems, such as those used for gas transport [43] (e.g., Baltic Pipe), to evaluate their vulnerability to underwater explosions. This research highlights the importance of protecting critical infrastructure against potential terrorist attacks and is planned as an extension of the work presented in [44], which already foresaw today's challenges as early as 2010. Future work will focus on enhancing numerical models to predict and mitigate damage in high-risk scenarios, contributing to improved safety standards and preventive measures.

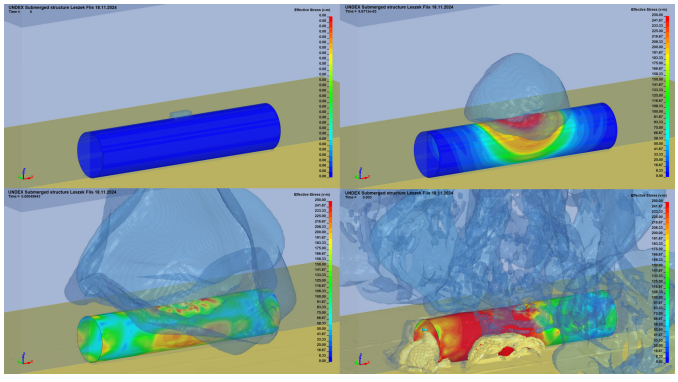

**Fig. 18.** Simulation of underwater pipeline systems, highlighting vulnerability to terrorist attacks and methods for improving resilience of critical infrastructure under UNDEX conditions (unit MPa)

Figure 19 depicts simulations of naval vessels under close-proximity explosions, addressing emerging threats from under-

water drones. The rise of unmanned underwater vehicles capable of delivering small explosive charges poses a significant challenge to ship safety. Unlike traditional scenarios requiring far-field explosions to damage a vessel, these drones can deliver precise close-range attacks, causing severe damage with relatively small explosive loads. Future research will prioritize the development of countermeasures and advanced detection systems to address these emerging threats effectively.

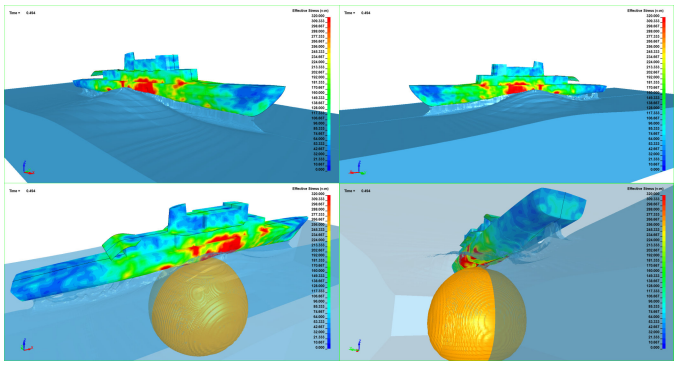

**Fig. 19.** Simulation of a naval vessel subjected to close-proximity UNDEX, emphasizing the threat posed by underwater drones equipped with small explosive charges (unit MPa)

By addressing these challenges, future research aims to develop robust methodologies for analyzing and mitigating the effects of underwater explosions. This work will enhance the safety of marine systems, improve the resilience of critical infrastructure, and provide a basis for addressing new and evolving threats.

## 5. SUMMARY

Simulations are an effective tool for analyzing underwater explosions (UNDEX), especially where experiments are difficult or impossible. They allow for detailed studies of close-range explosions and energy transfer mechanisms.

This study demonstrates that the simulation results align closely with theoretical predictions, validating the accuracy of the UNDEX model. Key phenomena, such as shockwave propagation, gas bubble pulsation, and cavitation, were effectively replicated, confirming the robustness of the applied numerical methods. These findings highlight the potential of simulations for detailed analyses of complex underwater explosion scenarios. This capability is particularly important for scenarios where experimental setups are restricted by logistical or physical constraints.

The results presented here form a solid foundation for expanding numerical research into more intricate cases, providing insights into structural responses under extreme conditions.

By integrating simulations with theoretical and experimental methods, this field can achieve a deeper understanding of underwater explosion dynamics. These advancements will not only improve structural safety in underwater environments but also strengthen applications in defense systems and engineering.

Although simulations and theory cannot replace experiments entirely, they now offer accurate insights into UNDEX scenarios at a much lower cost. Improving simulation fidelity requires more computing power, but this remains more feasible than large-scale testing.

## ACKNOWLEDGEMENTS

The article was co-financed by the state budget of Poland and awarded by the Minister of Science within the framework of the Excellent Science II Programme.

Computations were carried out using the computers of Centre of Informatics Tricity Academic Supercomputer & Network.

## REFERENCES

[1] R.H. Cole, “Underwater explosions,” 1948.

[2] T. L. Geers and K. S. Hunter, “An integrated wave-effects model for an underwater explosion bubble,” *J. Acoust. Soc. Am.*, vol. 111, no. 4, pp. 1584–1601, 2002.

[3] E. Brujan, K. Nahen, P. Schmidt, and A. Vogel, “Dynamics of laser-induced cavitation bubbles near an elastic boundary,” *J. Fluid Mech.*, vol. 433, pp. 251–281, 2001.

[4] G. Chertock, “Transient flexural vibrations of ship-like structures exposed to underwater explosions,” *J. Acoust. Soc. Am.*, vol. 48, no. 1B, pp. 170–180, 1970.

[5] T.A. Vernon, *Whipping response of ship hulls from underwater explosion bubble loading*. Defence Research Establishment Atlantic, 1986.

[6] K. Ramajeyathilagam and C. Vendhan, “Deformation and rupture of thin rectangular plates subjected to underwater shock,” *Int. J. Impact Eng.*, vol. 30, no. 6, pp. 699–719, 2004.

[7] Z. Zong, Y. Zhao, and H. Li, “A numerical study of whole ship structural damage resulting from close-in underwater explosion shock,” *Mar. Struct.*, vol. 31, pp. 24–43, 2013.

[8] H. Wang, X. Zhu, Y. S. Cheng, and J. Liu, “Experimental and numerical investigation of ship structure subjected to close-in underwater shock wave and following gas bubble pulse,” *Mar. Struct.*, vol. 39, pp. 90–117, 2014.

[9] N. Gan, X. Yao, L. Liu, W. Xiao, and X. Wang, “Research on overall damage characteristics of a hull girder under explosion bubble collapse,” *Ocean Eng.*, vol. 188, p. 106315, 2019.

[10] Z. He, Z. Chen, Y. Jiang, X. Cao, T. Zhao, and Y. Li, “Effects of the standoff distance on hull structure damage subjected to near-field underwater explosion,” *Mar. Struct.*, vol. 74, p. 102839, 2020.

[11] H. Li, X. Zheng, C. Zhang, Z. Mei, X. Bai, and K. Liu, “Sagging damage characteristics of hull girder with trapezoidal cross-section subjected to near-field underwater explosion,” *Def. Technol.*, vol. 21, pp. 1–13, 2023.

[12] Z. Zhang, Y. Wang, H. Zhao, H. Qian, and J. Mou, “An experimental study on the dynamic response of a hull girder subjected to near field underwater explosion,” *Mar. Struct.*, vol. 44, pp. 43–60, 2015.

[13] Y.S. Shin, J.M. Didoszak, and J.J. Lepe, “NPS Shock Team, Shock & Vibration Computational Laboratory,” 2009.

[14] K.G. Webster, "Investigation of close proximity underwater explosion effects on a ship-like structure using the multi-material arbitrary lagrangian eulerian finite element method," Ph.D. dissertation, Virginia Tech, 2007.

[15] U. S. Hydrographic Office. Preliminary Design Branch Bureau of Ships Navy Department 1 January 1949. Submarine report depth charge, bomb, mine, torpedo and gunfire damage including losses in action 7 december, 1941 to 15 august, 1945 volume II. War Damage Report No. 58 Printed By U. S. Hydrographic Office. Section XV behavior of Underwater Non-Contact Explosion. [Online]. Available: https://tiny.pl/9d9mkfkg (Accessed 2024-11-12).

[16] D.C. Campbell. (1943) Motions of a pulsating gas globe under water: A photographic study. [Online]. Available: https://dome.mit.edu/handle/1721.3/48114 (Accessed 2024-11-12).

[17] B. Szturomski, *Modeling the Interaction of an Underwater Explosion with a Ship Hull Using the Finite Element Method*. Polish Naval Academy of the Heroes of Westerplatte, 2023.

[18] Y.S. Shin, "Ship shock modeling and simulation for far-field underwater explosion," *Comput. Struct.*, vol. 82, no. 23-26, pp. 2211–2219, 2004.

[19] A. Zhang, M. Furen, L. Yunlong, L. Shuai, and W. Shiping, "Review of research on underwater explosion related to load characteristics and ship damage and protection," *Chin. J. Ship Res.*, vol. 18, no. 3, pp. 139–154, 2023.

[20] A. Grządziela, A. Załęska-Fornal, and M. Kluczyk, "The single degree of freedom simulation model of underwater explosion impact," *Arch. Acoust.*, vol. 45, no. 2, pp. 341–348, 2020.

[21] Z. He, Z. Du, L. Zhang, and Y. Li, "Damage mechanisms of full-scale ship under near-field underwater explosion," *Thin-Walled Struct.*, vol. 189, p. 110872, 2023.

[22] P. Nowak, A. Szlachta, T. Gajewski, P. Peksa, and P. Sielicki, "Small-scale underwater explosion in shallow-water tank," *Ocean Eng.*, vol. 288, p. 115894, 2023.

[23] X. Zhang, Z. He, Z. Du, J. Wang, Y. Jiang, and Y. Li, "Multi-peak phenomenon of large-scale hull structural damage under near-field underwater explosion," *Ocean Eng.*, vol. 283, p. 114898, 2023.

[24] T. Zhengpeng and L. Xiangyu, "Application of the sub-sea analysis (SSA) capability in numerical simulation of underwater explosion," *J. Phys.-Conf. Ser.*, vol. 1965, no. 1, p. 012042, 2021.

[25] N.A. Schneider and Y.S. Shin, "Ship shock trial modeling and simulation of uss winston s. churchill (ddg 81)," Citeseer, Tech. Rep., 2003.

[26] K. Haglund and A. Melander, "An eulerian finite element analysis of a structure subjected to an underwater explosion," Master's thesis, Lund University. Department of Mechanical Engineering Solid Mecjanics, 2023.

[27] J. Park, "A runge kutta discontinuous galerkin-direct ghost fluid (RKDG-DGF) method to near-field early-time underwater explosion (UNDEX) simulations," Ph.D. dissertation, Virginia Tech, 2008.

[28] J. Chung, Y. Seo, and Y.S. Shin, "Dynamic and whipping response of the surface ship subjected to underwater explosion: experiment and simulation," *Ships Offshore Struct.*, vol. 15, no. 10, pp. 1129–1140, 2020.

[29] J. Chung and Y.S. Shin, "Simulation of dynamic behaviour of high-speed catamaran craft subjected to underwater explosion," *Ships Offshore Struct.*, vol. 9, no. 4, pp. 387–403, 2014.

[30] L. Flis, "Estimating the shock resistance of a ship using computer simulation," *Logistics*, p. 650, 2014 (in Polish).

[31] J. Malachowski, "Effect of blast wave on chosen structure–numerical and experimental study," *Int. J. Math. Comput. Simul.*, vol. 2, no. 3, pp. 228–235, 2008.

[32] LSTC, "LS-DYNA Keyword User's Manual, Volume II: Material Models," 2024. [Online]. Available: https://www.lstc.com/download/manuals

[33] A. Rusinek, J.A. Rodríguez-Martínez, R. Pesci, and J. Capelle, "Experimental characterisation and modelling of the thermo-viscoplastic behaviour of steel aisi 304 within wide ranges of strain rate at room temperature," *J. Theor. Appl. Mech.*, vol. 48, no. 4, pp. 1027–1042, 2010.

[34] Y.S. Shin and I. Ham, "Damping modeling strategy for naval ship system," Monterey, California. Naval Postgraduate School, Tech. Rep., 2003.

[35] S. Rutgerson, "Damping summary," unpublished.

[36] J.H. Gordis and J.M. Didoszak, "Analysis of the complex exponential method for modal parameter estimation from fsst data," unpublished.

[37] R. Bishop, "A note on structural damping of ship hulls," *J. Sound Vib.*, vol. 56, no. 4, 1978.

[38] Y.W. Kwon and J.M. Didoszak, "Improved structural damping models in undex modeling and simulation," Naval Postgraduate School, Monterey, CA, Technical Report, July 2016.

[39] J.M. Didoszak, "Updated approach to shock failure assessment of shipboard equipment," Ph.D. dissertation, Monterey, CA; Naval Postgraduate School, 2019.

[40] J. Didoszak and Y. Kwon, "Failure assessment of ship-board equipment subjected to underwater explosions," *Multiscale and Multidisciplinary Modeling, Experiments and Design*, vol. 8, no. 1, p. 17, 2025.

[41] A. Zhang, "3d dynamic behavior of underwater explosion bubble [d]," *Harbin-Harbin Eng. Univ.*, pp. 2–5, 2006.

[42] Nagesh and N. Gupta, "Underwater explosion (undex) phenomenon and response of marine combatants to undex loading," *Mech. Solids*, vol. 58, no. 1, pp. 338–351, 2023.

[43] R. Kiciński and B. Szturomski, "Algorithm describing the pressure distribution from a non-contact underwater mine explosion,," *Bull. Milit. Univ. Technol.*, vol. 63, no. 4, pp. 101–112, 2014.

[44] J. Małachowski, *Modelowanie i badania interakcji ciało stałe–gaz przy oddziaływaniu impulsu ciśnienia na elementy konstrukcji rurociągu*. Bel Studio, 2010.